NASA/TP-2008-215534

Projectile and Lab Frame Differential Cross Sections for Electromagnetic Dissociation

John W. Norbury
Langley Research Center, Hampton, Virginia

Anne Adamczyk and Frank Dick
Worcester Polytechnic Institute, Worcester, Massachusetts

October 2008

The NASA STI Program Office . . . in Profile

Since its founding, NASA has been dedicated to the advancement of aeronautics and space science. The NASA Scientific and Technical Information (STI) Program Office plays a key part in helping NASA maintain this important role.

The NASA STI Program Office is operated by Langley Research Center, the lead center for NASA's scientific and technical information. The NASA STI Program Office provides access to the NASA STI Database, the largest collection of aeronautical and space science STI in the world. The Program Office is also NASA's institutional mechanism for disseminating the results of its research and development activities. These results are published by NASA in the NASA STI Report Series, which includes the following report types:

- TECHNICAL PUBLICATION. Reports of completed research or a major significant phase of research that present the results of NASA programs and include extensive data or theoretical analysis. Includes compilations of significant scientific and technical data and information deemed to be of continuing reference value. NASA counterpart of peer-reviewed formal professional papers, but having less stringent limitations on manuscript length and extent of graphic presentations.

- TECHNICAL MEMORANDUM. Scientific and technical findings that are preliminary or of specialized interest, e.g., quick release reports, working papers, and bibliographies that contain minimal annotation. Does not contain extensive analysis.

- CONTRACTOR REPORT. Scientific and technical findings by NASA-sponsored contractors and grantees.

- CONFERENCE PUBLICATION. Collected papers from scientific and technical conferences, symposia, seminars, or other meetings sponsored or co-sponsored by NASA.

- SPECIAL PUBLICATION. Scientific, technical, or historical information from NASA programs, projects, and missions, often concerned with subjects having substantial public interest.

- TECHNICAL TRANSLATION. English-language translations of foreign scientific and technical material pertinent to NASA's mission.

Specialized services that complement the STI Program Office's diverse offerings include creating custom thesauri, building customized databases, organizing and publishing research results ... even providing videos.

For more information about the NASA STI Program Office, see the following:

- Access the NASA STI Program Home Page at ***http://www.sti.nasa.gov***

- E-mail your question via the Internet to help@sti.nasa.gov

- Fax your question to the NASA STI Help Desk at (301) 621-0134

- Phone the NASA STI Help Desk at (301) 621-0390

- Write to:
  NASA STI Help Desk
  NASA Center for AeroSpace Information
  7115 Standard Drive
  Hanover, MD 21076-1320

NASA/TP-2008-215534

Projectile and Lab Frame Differential Cross Sections for Electromagnetic Dissociation

John W. Norbury
Langley Research Center, Hampton, Virginia

Anne Adamczyk and Frank Dick
Worcester Polytechnic Institute, Worcester, Massachusetts

National Aeronautics and
Space Administration

Langley Research Center
Hampton, Virginia 23681-2199

October 2008

Available from:

NASA Center for AeroSpace Information (CASI)
7115 Standard Drive
Hanover, MD 21076-1320
(301) 621-0390

National Technical Information Service (NTIS)
5285 Port Royal Road
Springfield, VA 22161-2171
(703) 605-6000

Contents

List of Figures

Abstract

Differential cross sections for electromagnetic dissociation in nuclear collisions are calculated for the first time. In order to be useful for three - dimensional transport codes, these cross sections have been calculated in both the projectile and lab frames. The formulas for these cross sections are such that they can be immediately used in space radiation transport codes. Only a limited amount of data exists, but the comparison between theory and experiment is good.

1 Introduction

The issue of protecting astronauts from cosmic radiation is becoming increasingly important with the current plans to establish a permanent human base on the Moon with a follow-on mission to Mars. During a Mars mission, astronauts will be exposed to cosmic radiation fields for several years. What is unique to cosmic radiation fields is the presence of heavy nuclei (up to and beyond Z=26) with energies of GeV and beyond. In calculating space radiation environments, it is therefore necessary to have a detailed knowledge of nucleus - nucleus collisions in the GeV energy region where the cosmic ray spectrum reaches a maximum.

Nucleus - nucleus collisions are mediated mainly by either the strong or electromagnetic (EM) force. A reaction proceeding via the EM force is often called Electromagnetic Dissociation (EMD). For few nucleon removal, EMD cross sections are just as important as strong interaction cross sections. Differential EMD cross sections are necessary because fully three-dimensional transport codes require energy and angular differential cross sections. A full theory of *differential* EMD cross sections has never been worked out. That is the goal of the present paper, which is an expanded version of Reference [1].

2 Photonuclear cross sections

Nucleus - nucleus electromagnetic cross sections require photonuclear cross sections as input. Therefore, in this section, we first discuss these simpler and more basic photonuclear processes. Included is a discussion of the differential photonuclear cross section, which will be important when determining the nucleus - nucleus differential EMD cross section. We also present a review of the total cross section parameterization, because this will be used in obtaining differential cross sections.

2.1 Compound nucleus

Some excellent references that discuss compound nucleus formation are Frobrich [2] (pp. 372, 322, 346), Preston [3] (pp. 514-515), Blatt and Weisskopf [4] (p. 368), Paul [5]

(pp. 220-224), Burcham and Jobes [6] (p. 189), de Benedetti [7], Bethe and Morrison [8], Harakeh and van der Woude [9], Satchler [10] (pp. 75, 249), Feshbach [11] (pp. 296, 309, 326), McCarthy [12] and Jackson [13] (p. 94).

An essential point emphasized by Burcham and Jobes [6] (p. 191) is that the compound nucleus is a true intermediate resonance state, so that the reaction proceeds according to

$$X + a \rightarrow C^* \rightarrow Y + b, \tag{1}$$

where C^* represents the intermediate compound nucleus, rather than a direct reaction

$$X + a \rightarrow Y + b. \tag{2}$$

This means that the kinematics are entirely different. For the direct reaction (2), one *cannot* form a double differential cross section $\frac{d^2\sigma}{dEd\Omega}$ for the final particle b. Instead, $\frac{d\sigma}{dE}$ and $\frac{d\sigma}{d\Omega}$ are *not* independent, but are functions of each other. However, for the compound nucleus reaction, an essential feature is that the compound nucleus "forgets" how it was formed after reaching statistical equilibrium. This means that it is a true intermediate state and one instead focuses on compound nucleus decay

$$C^* \rightarrow Y + b. \tag{3}$$

Here, the spectral and angular distributions will be *independent* of each other, so that one can now form the double differential cross section $\frac{d^2\sigma}{dEd\Omega}$ for the final particle b. In the simplest model, the angular distributions will be constant and the spectral distribution will represent the statistical thermal decay of a Boltzmann system. The book by Preston [3] contains one of the most useful discussions of the compound nucleus, and a discussion of $\frac{d^2\sigma}{dEd\Omega}$ for the compound nucleus decay can be found on pages 514 - 515.

2.2 Two - body final state

We now consider reactions involving two or three particles in the final state. Suppose we have a reaction with only two bodies in the final state, such as

$$1 + 2 \rightarrow 3 + 4\ , \tag{4}$$

where the number denotes the particle. An example of such a reaction is

$$\gamma + A \rightarrow A^* \rightarrow (A-1)_0 + N\ , \tag{5}$$

where γ denotes a photon, A denotes a parent nucleus, N denotes a nucleon, and $(A-1)_0$ denotes a daughter nucleus in its *ground state*. In this reaction, the incident photon excites the parent nucleus to a compound nucleus excited state denoted by A^*. The

excited parent compound nucleus decays directly to the ground state of the daughter, with the emission of a nucleon, as shown in figure 1.

2.3 Three - body final state

Now consider a three - body final state, such as

$$1 + 2 \rightarrow 3 + 4 + 5, \tag{6}$$

where the number denotes the particle. An example of such a reaction is

$$\gamma + A \rightarrow A^* \rightarrow (A-1)^* + N \rightarrow (A-1)_0 + \gamma + N. \tag{7}$$

In this reaction, the parent nucleus is excited to an intermediate compound nucleus state, but now it decays to an excited state of the daughter nucleus again with the emission of a nucleon. The excited daughter then decays to its ground state by emitting a photon. (It could also decay to another excited state and emit another photon.) As shown in figure 2, there will be a variety of excited daughter states that are possible to populate.

For photonuclear reactions, one can measure *both* $\frac{d\sigma}{dE_N}$ and $\frac{d\sigma}{d\Omega_N}$ for an emitted nucleon N. Equivalently, one can form $\frac{d^2\sigma}{dE_N d\Omega_N}$. If the reaction occurred via equation (5), then both differential cross sections cannot be determined. It is important to realize that both angular and spectral distributions are *only* possible when the photonuclear reaction involves a three - body final state as in equation (7). Alternatively, this reaction could be thought of as involving a two - body final state $\gamma + A \rightarrow (A-1)^* + N$ where the mass of the daughter nucleus $(A-1)^*$ is not fixed but can vary, because it can exist in many different excited states or energy levels as shown in figure 2. This means effectively that the mass of the excited daughter nucleus is not fixed. Thus, the energy of the emitted nucleon can *vary* allowing the formation of $\frac{d\sigma}{dE}$.

2.4 Angular distribution

In the simplest compound nucleus model, the photonuclear angular distribution is approximately isotropic [3, 5, 10, 14], meaning that the angular distribution is constant,

$$\frac{d\sigma_{\gamma A}(E_\gamma)}{d\Omega_N} = K \ , \tag{8}$$

where K is a constant. It is trivial to evaluate K from the total cross section because

$$\sigma_{\gamma A}(E_\gamma) = \int \frac{d\sigma_{\gamma A}(E_\gamma)}{d\Omega_N} \, d\Omega_N = 4\pi K. \tag{9}$$

Rearranging gives

$$K = \frac{\sigma_{\gamma A}(E_\gamma)}{4\pi} \ . \tag{10}$$

An isotropic angular distribution can be written as

$$\frac{d\sigma_{\gamma A}(E_\gamma)}{d\Omega_N} = \frac{\sigma_{\gamma A}(E_\gamma)}{4\pi} \ . \tag{11}$$

2.5 Spectral distribution

The energy level density in figure 2 can be approximated [2], [11] (p. 326) by a Boltzmann distribution

$$\rho(E) \sim e^{-E/k\Theta} \ , \tag{12}$$

with the nuclear temperature given by [2, 11]

$$k\Theta = \sqrt{\frac{d\ E_\gamma}{A_P}} \ . \tag{13}$$

where d is a constant, sometimes taken as $d = 10$. Here, Θ is the nuclear temperature and k is the Boltzmann constant. The photonuclear spectral distribution is parameterized as

$$\frac{d\sigma_{\gamma A}(E_\gamma)}{dE_N} = C\ T_N\ e^{-T_N/k\Theta} \ , \tag{14}$$

where T_N is the kinetic energy of the emitted nucleon. We write $\frac{d\sigma}{dE_N}$ instead of $\frac{d\sigma}{dT_N}$ because $dE_N = dT_N$. The total energy is given by $E_N = T_N + m_N$, where m_N is the nucleon mass. Also, note that we do *not* have $E_N e^{-E_N/k\Theta}$, because E_N begins at m_N rather than zero.

2.5.1 Useful integrals

In order to evaluate the constant C in the above expression for the spectral distribution, we shall need the following integrals [15], [16]

$$\int dx\ xe^{-ax} = -\frac{1+ax}{a^2}\ e^{-ax} \ , \tag{15}$$

$$\int dE\ Ee^{-E/k\Theta} = -k\Theta(E + k\Theta)\ e^{-E/k\Theta} \ , \tag{16}$$

and

$$\int_0^\infty dx\ x^n e^{-ax} = \frac{\Gamma(n+1)}{a^{n+1}} = \frac{n!}{a^{n+1}}\ , \tag{17}$$

$$\int_0^\infty dx\ xe^{-ax} = \frac{1}{a^2}\ , \tag{18}$$

$$\int_0^\infty dE\ Ee^{-E/k\Theta} = (k\Theta)^2\ . \tag{19}$$

However, we will need these integrals with different limits, such as a minimum or maximum energy, $E_{\rm min} = E_{\rm threshold}$ or $E_{\rm max}$. Thus, the following integrals will be useful. From reference [15], we obtain

$$\begin{aligned}\int_B^C dx\ xe^{-ax} &= \frac{1+aB}{a^2}\ e^{-aB} - \frac{1+aC}{a^2}\ e^{-aC} \\ &= \frac{1+aB}{a^2}\ e^{-aB}\ , \qquad \text{for C} = \infty \ \text{ and } \ \text{Re[a]} > 0.\end{aligned} \tag{20}$$

This reduces to the above result for $B = 0$ and $C = \infty$,

$$\begin{aligned}\int_{E_{\rm min}}^{E_{\rm max}} dE\ Ee^{-E/k\Theta} &= k\Theta(E_{\rm min} + k\Theta)e^{-E_{\rm min}/k\Theta} - k\Theta(E_{\rm max} + k\Theta)e^{-E_{\rm max}/k\Theta} \\ &= k\Theta(E_{\rm min} + k\Theta)e^{-E_{\rm min}/k\Theta}\ , \qquad \text{for } \ E_{\rm max} = \infty.\end{aligned} \tag{21}$$

2.5.2 Spectral distribution in terms of total cross section

The photonuclear spectral distribution is written in equation (14), where T_N is the kinetic energy of the emitted nucleon, and C is a constant determined by the requirement

$$\sigma_{\rm tot}(E_\gamma) = \int dE_N\ \frac{d\sigma_{\gamma A}(E_\gamma)}{dE_N}\ , \tag{22}$$

where $\sigma_{\rm tot}(E_\gamma)$ is the photonuclear total cross section. First, assume that the limits of integration are 0 and ∞. Then,

$$\sigma_{\rm tot}(E_\gamma) = \int_0^\infty dE_N\ \frac{d\sigma_{\gamma A}(E_\gamma)}{dE_N} = C\int_0^\infty dT_N\ T_N e^{-T_N/k\Theta} = C(k\Theta)^2\ , \tag{23}$$

giving

$$C = \frac{\sigma_{\rm tot}(E_\gamma)}{(k\Theta)^2}\ , \tag{24}$$

or

$$\frac{d\sigma_{\gamma A}(E_\gamma)}{dE_N} = \frac{\sigma_{\rm tot}(E_\gamma)}{(k\Theta)^2}\, T_N\, e^{-T_N/k\Theta}\,, \tag{25}$$

which is the photonuclear spectral distribution.

We see that this has the correct units, noting that the units of $k\Theta$ are MeV. (In units where $k \equiv 1$, Θ is in MeV. This is used in the computer codes for this work.) Equation (25) makes sense because the differential cross section is proportional to the total cross section times the probability of decay, $\frac{d\sigma}{dE_N} \sim \sigma\, e^{-T_N/k\Theta}$. See figures 2 and 3 of reference [17]. The more general calculation, with arbitrary limits T_{min} and T_{max}, yields

$$\begin{aligned}
\sigma_{\rm tot}(E_\gamma) &= \int_{E_{\rm min}}^{E_{\rm max}} dE_N\, \frac{d\sigma}{dE_N} = C \int_{E_{\rm min}}^{E_{\rm max}} dT_N\, T_N e^{-T_N/k\Theta} \\
&= C\left[k\Theta(T_{\rm min}+k\Theta)e^{-T_{\rm min}/k\Theta} - k\Theta(T_{\rm max}+k\Theta)e^{-T_{\rm max}/k\Theta}\right].
\end{aligned} \tag{26}$$

Rearranging gives

$$C = \frac{\sigma_{\rm tot}(E_\gamma)}{k\Theta(T_{\rm min}+k\Theta)e^{-T_{\rm min}/k\Theta} - k\Theta(T_{\rm max}+k\Theta)e^{-T_{\rm max}/k\Theta}}\,. \tag{27}$$

Substituting this value of C into equation (14) yields

$$\begin{aligned}
\frac{d\sigma}{dE_N} &= \frac{\sigma_{\rm tot}(E_\gamma)}{k\Theta(T_{\rm min}+k\Theta)e^{-T_{\rm min}/k\Theta} - k\Theta(T_{\rm max}+k\Theta)e^{-T_{\rm max}/k\Theta}}\, T_N\, e^{-T_N/k\Theta} \\
&= \frac{\sigma_{\rm tot}(E_\gamma)}{k\Theta(T_{\rm min}+k\Theta)e^{-T_{\rm min}/k\Theta}}\, T_N\, e^{-T_N/k\Theta}\,, \qquad \text{for } T_{\rm max} = \infty.
\end{aligned} \tag{28}$$

This reduces to the above result, equation (25), when $T_{\rm min} = 0$ and $T_{\rm max} = \infty$.

2.6 Double differential cross section

From reference [14] (pp. 27, 40) (with $f = 0$), the photonuclear double differential cross section can be expressed as

$$\frac{d^2\sigma_{\gamma A}(E_\gamma)}{dE_N d\Omega_N} = \frac{1}{4\pi}\frac{d\sigma_{\gamma A}(E_\gamma)}{dE_n}\,, \tag{29}$$

which corresponds to an isotropic angular distribution.

2.7 Lorentz invariant differential cross section

The Lorentz invariant differential cross section $E\frac{d^3\sigma}{d^3p}$ is related to the non-invariant double differential cross section via

$$E_N \frac{d^3\sigma_{\gamma A}(E_\gamma)}{d^3p_N} = \frac{1}{p_N} \frac{d^2\sigma_{\gamma A}(E_\gamma)}{dE_N d\Omega_N} \,, \tag{30}$$

where $p_N \equiv |\mathbf{p}_N|$. Note that the entire right hand side is to be evaluated in the *same* frame. For example, if the double differential cross section $\frac{d^2\sigma}{dE_N d\Omega_N}$ is evaluated in the projectile frame, then the term $\frac{1}{p_N}$ also refers to the projectile frame. If the angular distribution is isotropic, we have

$$E_N \frac{d^3\sigma_{\gamma A}(E_\gamma)}{d^3p_N} = \frac{1}{4\pi p_N} \frac{d\sigma_{\gamma A}(E_\gamma)}{dE_N} \,. \tag{31}$$

2.8 Total cross section

The above equations for the photonuclear differential cross sections were all written in terms of the photonuclear total cross section. We now present relevant equations to calculate the photonuclear total cross section. The photonuclear total cross section for producing particle X is [18, 19]

$$\sigma(E_\gamma, X) = g_X \sigma_{\rm abs}(E_\gamma) \,, \tag{32}$$

where g_X is the branching ratio and $\sigma_{\rm abs}(E_\gamma)$ is the photonuclear absorption cross section, which is parameterized as

$$\sigma_{\rm abs}(E_\gamma) = \frac{\sigma_m}{1 + \left[(E_\gamma^2 - E_{\rm GDR}^2)^2 / E_\gamma^2 \Gamma^2\right]} \,. \tag{33}$$

The abbreviation, GDR, stands for giant dipole resonance. Here, $E_{\rm GDR}$ is the energy at which the photonuclear cross section has its peak value and Γ is the width of the electric dipole (E1) giant dipole resonance. Also,

$$\sigma_m = \frac{\sigma_{\rm TRK}}{\pi\Gamma/2} \,, \tag{34}$$

with the Thomas-Reiche-Kuhn cross section given by [19]

$$\sigma_{\rm TRK} = \frac{60 N_P Z_P}{A_P} \text{ MeV mb} \,, \tag{35}$$

with the subscript P referring to excitation of the projectile. (Note that in reference [19] a typing error had this subscript referring to the target.) The GDR energy is

$$E_{\rm GDR} = \frac{\hbar c}{\left[\frac{m^* c^2 R_0^2}{8J}(1 + u - \frac{1+\epsilon+3u}{1+\epsilon+u}\,\epsilon)\right]^{1/2}} \,, \tag{36}$$

with

$$u = \frac{3J}{Q'} A_P^{-1/3} \,, \tag{37}$$

and

$$R_0 = r_0 A_P^{1/3}. \tag{38}$$

(In reference [19] a typing error had this subscript referring to the target.) The parameters are:

$$\begin{aligned} \epsilon &= 0.0768 \,, & (39)\\ Q' &= 17 \text{ MeV} \,, & (40)\\ J &= 36.8 \text{ MeV} \,, & (41)\\ r_0 &= 1.18 \text{ fm} \,, & (42)\\ m^* &= 0.7\, m_{\rm nucleon} \,. & (43) \end{aligned}$$

3 Nucleus - nucleus cross sections

In a nucleus - nucleus collision mediated by the EM force, the target (or projectile) represents a source of virtual photons, which impinge upon the projectile (or target). The spectrum of virtual photons contains a variety of energies, in contrast to a photonuclear reaction where the incoming photon possesses only a single energy. For a nucleus - nucleus collision, figures 1 and 2 get replaced by figures 3 and 4, which show a variety of energy levels being excited in the parent nucleus.

3.1 Total cross section

The total cross section for nucleus - nucleus reactions can be written in the form

$$\sigma_{AA} = \int dE_\gamma \; N(E_\gamma)\; \sigma_{\gamma A}(E_\gamma) \,, \tag{44}$$

where $N(E_\gamma)$ is the Weiszacker-Williams virtual photon spectrum and $\sigma_{\gamma A}(E_\gamma)$ is the photonuclear total cross section.

3.2 Angular distribution

From the perspective of EMD reactions, the spectator nucleus is nothing more than a source of virtual photons, therefore the angular and spectral distributions may also be written in the form of equation (44). Thus, the angular distribution, for emission of a nucleon N in the direction Ω_N, is given by

$$\frac{d\sigma_{AA}}{d\Omega_N} = \int dE_\gamma \; N(E_\gamma) \; \frac{d\sigma_{\gamma A}(E_\gamma)}{d\Omega_N} \; , \tag{45}$$

where $\frac{d\sigma_{\gamma A}(E_\gamma)}{d\Omega_N}$ is the photonuclear angular distribution for emission of a nucleon N in the direction Ω_N. If the photonuclear angular distribution is approximately isotropic, then use of equations (11) and (45) gives

$$\frac{d\sigma_{AA}}{d\Omega_N} = \frac{\sigma_{AA}}{4\pi} \; . \tag{46}$$

It must be emphasized that this is the angular distribution in the *rest frame of the compound nucleus*. If the compound nucleus is the projectile, then this must be transformed to the lab frame for use in transport codes. If the compound nucleus is the target, then no transformation is necessary, because the target is at rest in the lab frame.

3.3 Spectral distribution

The spectral distribution, for emission of a nucleon N with energy E_N, may also be written in the form of equation (44), namely

$$\frac{d\sigma_{AA}}{dE_N} = \int dE_\gamma \; N(E_\gamma) \; \frac{d\sigma_{\gamma A}(E_\gamma)}{dE_N} \; , \tag{47}$$

where $\frac{d\sigma_{\gamma A}(E_\gamma)}{dE_N}$ is the photonuclear spectral distribution for emission of a nucleon N with energy E_N. *Note that the spectral distribution cannot be taken outside the integral because the nuclear temperature Θ depends on the photon excitation energy E_γ.*

3.4 Double differential cross section

The double differential cross section, for emission of a nucleon N with energy E_N in the direction Ω_N, may also be written in the form of equation (44), namely

$$\frac{d^2\sigma_{AA}}{d\Omega_N dE_N} = \int dE_\gamma \; N(E_\gamma) \; \frac{d^2\sigma_{\gamma A}(E_\gamma)}{d\Omega_N dE_N} \; , \tag{48}$$

where $\frac{d^2\sigma_{\gamma A}(E_\gamma)}{d\Omega_N dE_N}$ is the photonuclear double differential cross section for emission of a nucleon N with energy E_N in the direction Ω_N. If the photonuclear angular distribution is isotropic, we use equation (29) to give

$$\begin{aligned} \frac{d^2\sigma_{AA}}{d\Omega_N dE_N} &= \frac{1}{4\pi}\int dE_\gamma\ N(E_\gamma)\ \frac{d\sigma_{\gamma A}(E_\gamma)}{dE_N} \\ &= \frac{1}{4\pi}\frac{d\sigma_{AA}}{dE_N}\ , \end{aligned} \tag{49}$$

which is analogous to equation (29).

3.5 Lorentz invariant differential cross section

The Lorentz invariant differential cross section is related to the non-invariant double differential cross section as before, namely

$$E_N\frac{d^3\sigma_{AA}}{d^3p_N} = \frac{1}{p_N}\ \frac{d^2\sigma_{AA}}{dE_N d\Omega_N}\ . \tag{50}$$

For an isotropic distribution, we have the analog of equation (31),

$$E_N\frac{d^3\sigma_{AA}}{d^3p_N} = \frac{1}{4\pi p_N}\ \frac{d\sigma_{AA}}{dE_N}\ . \tag{51}$$

4 Lorentz transformation of cross sections

The nucleus - nucleus differential cross sections in equations (45), (47), (48) all involve a photonuclear differential cross section or a total cross section. The photonuclear differential cross sections are all evaluated in the rest frame of the nucleus undergoing the photonuclear reaction. Differential cross sections in radiation transport codes are required in the lab frame (spacecraft rest frame). If the projectile nucleus is undergoing photodisintegration, then the nucleus - nucleus differential cross sections in equations (45), (47), (48) are first evaluated in the projectile frame. Then, they must be Lorentz transformed to the lab frame. The technique for doing this is the subject of the present section.

4.1 Discussion of photonuclear cross sections

For a two - body final state, such as the reaction in equation (5), one can form *either* the angular *or* spectral distribution, but not both. A double differential cross section or Lorentz invariant differential cross section cannot be formed in this case. For a three - body final state, such as the reaction in equation (7), both the spectral and angular distributions

can be formed independently, as well as double and Lorentz invariant differential cross sections. This can be seen in the literature for photonuclear reactions.

For general photonuclear reactions, numerous discussions of double differential cross sections [17], [20] - [27] can be found. However, for photonuclear reactions to the ground state, one can find information regarding only angular distributions [28] - [31]. This result is expected because when making a transition to the ground state, as shown in figure 1, there will be no energy distribution for the emitted nucleon when assuming the incident photon is monoenergetic. This is true for *any* transition to a *particular* energy state in the daughter nucleus. Although, when one allows for transitions to a variety of energy states in the daughter, as shown in figure 2, there will then be a variety of possible emitted nucleon energies whose spectral distribution will reflect the energy level density of the daughter nucleus. A transition to the ground state of the daughter nucleus is distinctive because no photon is emitted, and the final state will be a two - body state. Consequently, the angular distribution calculated in the projectile frame will need to be transformed into the lab frame, which is a complicated task.

From the view of a statistical compound nucleus decay, there is nothing special about the ground state. It is just one of a continuum of possible final states, which is given by the continuous energy level distribution $\rho(E)$. In this general case, the final state is three - body. This enables the formation of a Lorentz invariant differential cross section, which is easily transformed from the projectile to the lab frame. (Even though $E\frac{d^3\sigma}{d^3p}$ is invariant, it must be transformed when plotting it as a function of energy or angle.)

4.2 Lorentz transformation of photonuclear cross sections

A Lorentz transformation of a photonuclear differential cross section is almost never considered because it is inherently defined in the rest frame of the nucleus, which undergoes the reaction. The projectile is a photon, the target is a nucleus, and Lorentz transformation is not necessary. When considering *nucleus* - *nucleus* collisions, Lorentz transformations are needed. Assume that the projectile nucleus is undergoing the photonuclear reaction. Now, we *must* transform the projectile photonuclear differential cross section into the target nucleus frame.

In this section, when a Lorentz transformation of a differential photonuclear cross section is discussed, we are considering the different frames available to the nucleus - nucleus reaction, not the photonuclear reaction. This is admittedly a confusing point. It is important to realize that the photonuclear reaction is still occurring to the projectile nucleus. Normally, we would just integrate the projectile photonuclear cross section over the virtual photon spectrum coming from the target nucleus. We still do this, but first we transform the projectile photonuclear cross section to the lab (target) frame. It should be noted that although the photonuclear cross sections are transformed to the lab frame and written in terms of lab variables, they are still photonuclear cross sections for projectile fragmentation.

4.3 Lorentz transformation between cm or projectile frame and lab (target) frame

Suppose we have quantities in the center of momentum (cm) or projectile frames and we wish to transform to the lab frame. *The cm frame moves at speed β_{cl} relative to the lab frame.* The corresponding γ factor is labeled as γ_{cl}. *The projectile frame moves at speed β_{pl} relative to the lab frame.* The corresponding γ factor is labeled as γ_{pl}. The Lorentz transformations are

$$\begin{pmatrix} E_* \\ p_{||*} \end{pmatrix} = \begin{pmatrix} \gamma_{*l} & -\gamma_{*l}\beta_{*l} \\ -\gamma_{*l}\beta_{*l} & \gamma_{*l} \end{pmatrix} \begin{pmatrix} E_l \\ p_{||l} \end{pmatrix}, \quad p_{T*} = p_{Tl} \ , \tag{52}$$

and inverse transformations are

$$\begin{pmatrix} E_l \\ p_{||l} \end{pmatrix} = \begin{pmatrix} \gamma_{*l} & \gamma_{*l}\beta_{*l} \\ \gamma_{*l}\beta_{*l} & \gamma_{*l} \end{pmatrix} \begin{pmatrix} E_* \\ p_{||*} \end{pmatrix}, \quad p_{Tl} = p_{T*} \ , \tag{53}$$

where

$$p_{||} \equiv p_z = |\mathbf{p}| \cos\theta \ , \tag{54}$$

$$p_T = |\mathbf{p}| \sin\theta. \tag{55}$$

With this notation, both cm and projectile frames are included. The notation means that a quantity x_* is the value of the quantity x *evaluated in that particular frame* with

$$* = c \quad \text{or} \quad * = p, \tag{56}$$

where the c or p subscript refers to the cm or projectile frame, respectively, and β_{*l} is the speed of that frame *with respect to the lab frame* with

$$\beta_{*l} = \beta_{cl} \quad \text{or} \quad \beta_{*l} = \beta_{pl}. \tag{57}$$

4.4 Energy transformations

The energy Lorentz transformation from the lab (l) frame to the starred ($*$) frame is

$$\begin{aligned} E_{j*} &= \gamma_{*l}(E_{jl} - \beta_{*l} p_{||jl}) \\ &= \gamma_{*l}(E_{jl} - \beta_{*l} |\mathbf{p}_{jl}| \cos\theta_{jl}) \\ &= \gamma_{*l}\left(E_{jl} - \beta_{*l}\sqrt{E_{jl}^2 - m^2}\cos\theta_{jl}\right). \end{aligned} \tag{58}$$

The inverse transformation is

$$E_{jl} = \gamma_{*l}\left(E_{j*} + \beta_{*l}\sqrt{E_{j*}^2 - m^2}\cos\theta_{j*}\right). \tag{59}$$

4.5 Angle transformations

The angle is obtained from

$$\tan\theta = \frac{p_T}{p_z} \ . \tag{60}$$

Thus, the angle of particle j is

$$\begin{aligned} \tan\theta_{jl} = \frac{p_{T\,jl}}{p_{z\,jl}} &= \frac{p_{T\,j*}}{\gamma_{*l}\beta_{*l}E_{j*} + \gamma_{*l}p_{z\,j*}} \\ &= \frac{|\mathbf{p}_{j*}|\sin\theta_{j*}}{\gamma_{*l}\left(\beta_{*l}E_{j*} + |\mathbf{p}_{j*}|\cos\theta_{j*}\right)} \ . \end{aligned} \tag{61}$$

Defining α_{j*} as the speed of the cm or projectile frame relative to the lab frame divided by the speed of particle j in the cm or projectile frame

$$\alpha_{j*} \equiv \frac{\beta_{*l}}{\beta_{j*}} \ , \tag{62}$$

and using

$$\beta_{j*} = \frac{|\mathbf{p}_{j*}|}{E_{j*}} \ , \tag{63}$$

we obtain

$$\tan\theta_{jl} = \frac{\sin\theta_{j*}}{\gamma_{*l}\left(\cos\theta_{j*} + \alpha_{j*}\right)} \ . \tag{64}$$

See references [32] (p. 402), [33] (p. 42), [34] (p. 17), [35] (p. 26). This is a complicated function of θ because, in general,

$$\alpha_{j*} = \alpha_{j*}(E_{j*}) = \alpha_{j*}(\theta_{j*}). \tag{65}$$

Usually, α_{j*} is a function of θ_{j*}, making $\tan\theta_{jl}$ *a complicated function of θ_{j*}. For the cm frame and for three - body states, however, E_{jc} is not a function of θ_{jc}. This means that α_{jc} is not a function of θ_{jc} [33] (pp. 42, 58).* Three - body states are considered in the present work, so that we avoid the aforementioned complications.

The angle transformation for $* = c$ is plotted in references [32] (p. 403), [33] (p. 43), [36]). When $\alpha_{j*} > 1$, the function is double valued. This results from the two different angles in the cm or projectile frame giving rise to the same angle in the lab frame for $\alpha_{j*} > 1$. The two angles can be distinguished by their energies, labeled in the cm frame as $E_{jc}^{\pm}$ [32] (p. 402). This is true for a two - body final state.

To show that the cm or projectile angle is double valued, we specify the $*$ frame in equation (64) to be the projectile frame. Then,

$$\tan\theta_{jl} = \frac{\sin\theta_{jp}}{\gamma_{pl}\left(\cos\theta_{jp} + \alpha_{jp}\right)}, \tag{66}$$

where α_{jp} is defined as the ratio of the projectile velocity to the velocity of particle j in the projectile system. It is dependent on the lab kinetic energy T_N, as in $\alpha_{jp}(T_N)$. When $\alpha_{jp} > 1$, particles are emitted forwards and backwards in the projectile system, but appear at the same lab angle. Figures 5 - 8 are evaluated at the lab kinetic energy of m_N, $10m_N$, $16m_N$, and $100m_N$, respectively. Figures 5 and 6 are examples of what happens when $\alpha_{jp} > 1$. It can be seen that the range of the lab angle, $0 \leq \theta_{lab} \leq \theta_{max}$, is dependent on α_{jp}. The lab angle is also confined to a forward cone, as the projectile angle ranges from 0 to π. This means that the projectile angle will be double valued for every lab angle. Figures 7 and 8, however, illustrate the relationship between the projectile angle and the lab angle when $\alpha_p < 1$. Notice that the lab angle range is now between 0 and π. The lab angle is now a single valued function of the projectile angle.

In the present work, we consider three - body final states. The curves plotted in reference [32] (p. 403) correspond to a particular value of the particle energy, or in other words, to a particular value of α_{j*}. For a three - body reaction, the energy of the emitted particle is *not* related to the angle. Thus, for a particular lab angle, we have a continuous range of lab energies corresponding to a *family* of curves. This is plotted in reference [32] (p. 403). The family of curves will be for both $\alpha > 1$ and $\alpha < 1$.

The inverse transformation is

$$\tan\theta^{\pm}_{j*} = \frac{\sin\theta_{jl}}{\gamma_{*l}(\cos\theta_{jl} - \alpha^{\pm}_{jl})}\ , \tag{67}$$

where

$$\beta^{\pm}_{jl} = \frac{|\mathbf{p}^{\pm}_{jl}|}{E^{\pm}_{jl}}\ , \tag{68}$$

$$\alpha^{\pm}_{jl} \equiv \frac{\beta_{*l}}{\beta^{\pm}_{jl}}\ . \tag{69}$$

The $\pm$ notation is emphasizing that, in general, two different angles in the cm or projectile frames can correspond to a single angle in the lab frame.

4.6 Double differential cross sections

The transformation of a double differential cross section is described in reference [37]. The cross sections are related by the Jacobian

$$\frac{d^2\sigma}{dE_{jl}d\Omega_{jl}} = \frac{d^2\sigma}{dE_{j*}d\Omega_{j*}} \frac{\partial(E_{j*},\Omega_{j*})}{\partial(E_{jl},\Omega_{jl})} \,, \tag{70}$$

which is evaluated as

$$\frac{\partial(E_*,\Omega_*)}{\partial(E_l,\Omega_l)} = \frac{|\mathbf{p}_l|}{|\mathbf{p}_*|} = \frac{\sin\theta_*}{\sin\theta_l} \,, \tag{71}$$

to give

$$\frac{d^2\sigma}{dE_{jl}d\Omega_{jl}} = \frac{|\mathbf{p}_l|}{|\mathbf{p}_*|} \frac{d^2\sigma}{dE_{j*}d\Omega_{j*}} = \frac{\sin\theta_{j*}}{\sin\theta_{jl}} \frac{d^2\sigma}{dE_{j*}d\Omega_{j*}} \,. \tag{72}$$

The left hand side is a function of E_{jl} and θ_{jl}, so that the right hand side also should be function of E_{jl} and θ_{jl}. This is accomplished by replacing E_{j*} and θ_{j*} on the right hand side with equations (58) and (67). *Thus, the entire right hand side is written as an explicit function of lab variables.* We have written two versions of the right hand side. Either version can be used, and the one involving the sine functions will be a good test of the correctness of the angle transformations.

Equation (72) is the equation for obtaining all cross sections in the lab frame. The method is to use equation (72) to obtain the photonuclear double differential cross section in the lab frame. Then integrate the lab frame double differential cross section in equation (72), to get the photonuclear spectral and angular differential cross sections in the lab frame. To obtain any nucleus - nucleus differential cross section in the lab frame, take the lab frame photonuclear cross sections and integrate over the virtual photon spectrum.

5 Results

The results of these calculations are presented in figures 9 - 22. The photonuclear differential cross sections are presented in figures 9 - 14, which are evaluated at a photon energy of 20 MeV, near the peak of a typical giant resonance. The nucleus - nucleus differential cross sections are presented in figures 15 - 20. The cross sections in figures 9 - 20 are for the reaction

$$^{28}\mathrm{Si} + {}^{208}\mathrm{Pb} \rightarrow \mathrm{n} + {}^{27}\mathrm{Si} + {}^{208}\mathrm{Pb} \tag{73}$$

at 14.6 AGeV. Figure 9 shows the application of equation (25) to calculate the photonuclear spectral distribution in the lab frame. Equation (11) was used to calculate an isotropic photonuclear angular distribution in the lab frame, as seen in figure 10. The

photonuclear double differential cross section in the lab frame is given by equation (29) and is shown in figure 11.

These photonuclear cross sections are transformed to the nucleus - nucleus lab frame and are shown in figures 12 - 14. The photonuclear double differential cross section in the lab frame, as shown in figure 12, displays the double peak feature discussed by Hagedorn [38] (pp. 47 - 49). This double peak occurs because there is a single peak in the spectral distribution in the projectile frame (figure 9), which gets boosted both forward and backward in the lab frame depending on kinematic conditions. Figure 13 displays the photonuclear spectral distribution in the lab frame, which results from integrating the photonuclear double differential cross section in the lab frame over all lab angles. Compared to figure 9, it can be seen that the nucleon kinetic energies receive a large boost because of the high energy of the projectile. The angular distribution in the lab frame is obtained by integrating the photonuclear double differential cross section in the lab frame over all lab energies. In the projectile frame, the photonuclear angular distribution is isotropic; while in the lab frame it becomes non-isotropic and is peaked strongly in the forward direction. These features of the photonuclear angular distribution in the lab frame can be observed in figure 14.

The nucleus - nucleus differential cross sections are obtained by taking the corresponding photonuclear cross section and integrating over the virtual photon spectrum, as discussed previously. It can be seen that all the nucleus - nucleus differential cross sections, in both the projectile and lab frames, follow the shapes of the corresponding photonuclear differential cross sections. This makes sense because the photonuclear differential cross sections are just integrated over the virtual photon spectrum. In the lab frame, the nucleus - nucleus differential cross sections, just like for the photonuclear differential cross sections, have nucleon kinetic energies that receive a large boost and angles that strongly peak in the forward direction.

6 Comparison to experiment

There is very little experimental data concerning differential cross sections for electromagnetic dissociation. The best data available has been measured by Barrette *et al.* [39, 40], but much of their data involved spectral distributions of excitation energy. This will be analyzed in future work. However, a notable feature of their measurements is that *all of their angular distributions are approximately isotropic in the projectile frame, which agrees with the assumption of the present work.* Some kinetic energy distributions have been measured for outgoing neutrons and protons. See figure 13 of Barrette *et al.* [40]. In figures 21 and 22, we have compared our theory to these data. There are two points to note about these figures. Firstly, the experimental work quoted arbitrary units, so it was necessary to fit the absolute value (peak cross section) to the experiment. Secondly, the best fit is obtained by choosing the nuclear temperature constant in equation (13) as

$d = 20$. The comparison between theory and the limited experimental data is good. A better fit can probably be obtained with a more sophisticated approach to calculating the nuclear temperature and the spectral distribution (25).

7 Conclusions

This paper presents the first calculations of differential cross sections for electromagnetic dissociation in nucleus - nucleus collisions. These cross sections will be used in three - dimensional transport codes to improve estimates of radiation dose inside spacecraft. The results are given in a form in which they can be immediately used in fully three-dimensional space radiation transport codes that require differential cross sections in the lab frame. Cross sections are isotropic in the projectile frame and are in agreement with experiment. Spectral distributions in the projectile frame are compared to experimental results and are found to be in good agreement. However, the amount of data availble is very limited and the acquisition of more data would be very useful. Future work will involve a more sophisticated approach to calculating the spectral distribution and the nuclear temperature.

References

[1] J. W. Norbury and A. Adamczyk, Nuclear Instruments and Methods in Physics Research B, **254**, 177 (2007).

[2] P. Frobrich and R. Lipperheide, *Theory of nuclear reactions* (Clarendon Press, Oxford, 1996).

[3] M. A. Preston, *Physics of the Nucleus* (Addison-Wesley, Reading, Massachusetts, 1962).

[4] J. W. Blatt, and V. F. Weisskopf, *Theoretical nuclear physics* (Dover Publications, New York, 1991).

[5] E. B. Paul, *Nuclear and particle physics* (Wiley, New York, 1969).

[6] W. E. Burcham, and M. Jobes, *Nuclear and particle physics* (Longman Scientific and Technical, New York, 1994).

[7] S. DeBenedetti, *Nuclear interactions* (Wiley, New York, 1964).

[8] H. A. Bethe and P. Morrison, *Elementary nuclear theory*, Second edition (Wiley, New York, 1956).

[9] M. N. Harakeh and A. van der Woude, *Giant resonances*, (Clarendon Press, Oxford, 2001).

[10] G. R. Satchler, *Introduction to nuclear reactions*, Second edition (Macmillan Education Ltd., New York, 1990).

[11] H. Feshbach, *Theoretical nuclear physics* (Wiley, New York, 1992).

[12] I. E. McCarthy, *Nuclear reactions* (Pergamon Press, New York, 1970).

[13] D. F. Jackson, *Nuclear reactions* (Metheun and Co., London, 1970).

[14] *Handbook on photonuclear data for applications - cross sections and spectra*, IAEA-TECDOC-Draft No.3. (March 2000).

[15] S. Wolfram, *The Mathematica book* (Wolfram Research Inc., Champaign, Illinois, 2006).

[16] M. R. Spiegel, *Mathematical handbook* (Mc-Graw-Hill, New York, 1995).

[17] V. G. Shevchenko and B. A. Yuryev, Nuclear Physics, **37**, 495 (1962).

[18] P. Frobrich and R. Lipperheide, *Theory of nuclear reactions*, (Clarendon Press, Oxford, 1996).

[19] J. W. Norbury and L. W. Townsend. *Electromagnetic Dissociation Effects in Galactic Heavy-Ion Fragmentation*. NASA Technical Paper, NASA TP-2527 (1986).

[20] M. B. Chadwick, P. G. Young, R. E. MacFarlane, M. C. White, and R. C. Little, Nuclear Science and Engineering, **144**, 157 (2003).

[21] M. B. Chadwick, P. G. Young, and S. Chiba, Journal of Nuclear Science and Technology, **32**, 1154 (1995).

[22] J. C. McGeorge, G. I. Crawford, R. Owens, M. R. Sene, D. Branford, A. C. Shotter, B. Schoch, R. Beck, P. Jennewein, F. Klein, J. Vogt, and F. Zettl, Physics Letters B, **179**, 212 (1986).

[23] J. R. Wu and C. C. Chang, Physical Review C, **16**, 1812 (1977).

[24] W. A. Butler and G. B. Almy, Physical Review, **91**, 58 (1953).

[25] B. C. Diven and G. M. Almy, Physical Review, **80**, 407 (1950).

[26] G. A. Price, Physical Review, **93**, 1279 (1954).

[27] P. A. Tipler and R. A. Llewellyn, *Modern physics*, 3rd ed., (Freeman, New York, 1999).

[28] J. E. E. Baglin, and M. N. Thomson, Nuclear Physics A, **138**, 11 (1965).

[29] J. W. Jury, C. K. Ross, and N. K. Sherman, Nuclear Physics A, **337**, 503 (1980).

[30] Y. Birenbaum, Z. Berant, S. Kahane, and A. Wolf, Nuclear Physics A, **369**, 483 (1981).

[31] J. G. Woodworth, K. G. McNeill, J. W. Jury, P. D. Georgopulos, and R. G. Johnson, Nuclear Physics A, **327**, 53 (1979).

[32] J. D. Jackson, *Classical electrodynamics*, First edition (Wiley, New York, 1972).

[33] E. Byckling and K. Kajantie, *Particle kinematics* (Wiley, New York, 1973).

[34] M. Leon, *Particle physics: An introduction* (Academic Press, New York, 1973).

[35] C. J. Joachain. *Quantum collisions theory* (North-Holland, Amsterdam, 1983).

[36] K. G. Dedrick, *Kinematics of high-energy particles*, Rev. Mod. Phys. **34** pp. 429-442 (1962).

[37] J. W. Norbury and F. Dick, *Differential cross section Kinematics for 3-dimensional Transport Codes*. NASA Technical Paper (in press).

[38] R. Hagedorn, *Relativistic kinematics* (Benjamin, New York, 1963).

[39] J. Barrette, *et al.*, Physical Review C, **45**, 2427 (1992).

[40] J. Barrette, *et al.*, Physical Review C, **51** , 865 (1995).

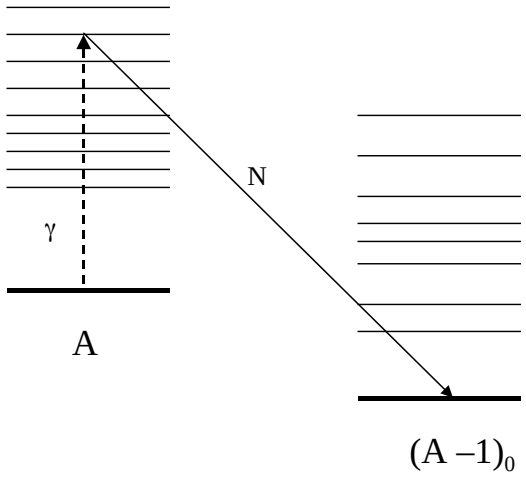

Figure 1: Photonuclear reaction with a two - body final state via the reaction $\gamma + A \rightarrow (A-1)_0 + N$. This shows the decay of an excited parent nucleus, with nucleon emission, to the ground state of the daughter nucleus. The parent is excited to only one energy level E, which is determined by the incident photon of energy E_γ in the photonuclear reaction. The energy of the emitted nucleon is fixed.

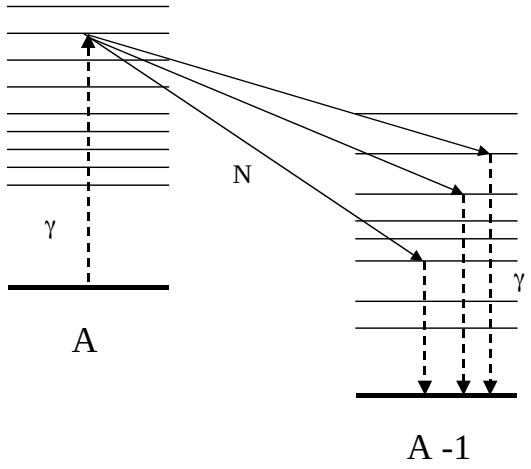

Figure 2: Photonuclear reaction with a three - body final state, $\gamma + A \rightarrow (A-1) + \gamma + N$. This shows the decay of an excited parent nucleus, with nucleon emission, to a variety of energy levels in the excited daughter nucleus. The parent is excited to only one energy E, which is determined by the incident photon of energy E_γ in the photonuclear reaction. The energy level distribution $\rho(E)$ in the daughter nucleus gives rise to a variety of energies E for the emitted nucleon, which gives rise to the Boltzmann distribution $e^{-E/k\Theta}$.

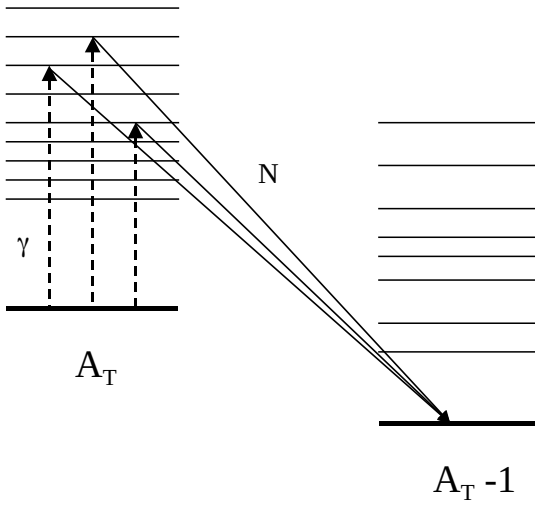

Figure 3: Nucleus - nucleus reaction, $A_P + A_T \rightarrow A_P + (A_T - 1) + N$. This shows the decay of an excited parent target nucleus, with nucleon emission, to the ground state of the daughter nucleus. The parent can be excited to a variety of energies because the projectile nucleus A_P brings in a variety of incident photon energies. The energy of the emitted nucleon can vary.

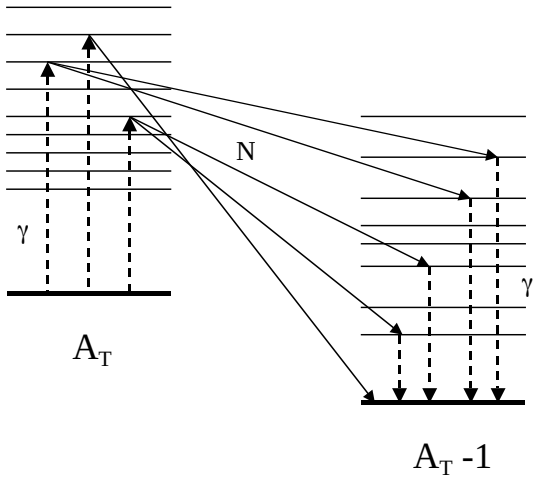

Figure 4: Nucleus - nucleus reaction, $A_P + A_T \rightarrow A_P + (A_T - 1) + N$. This shows the decay of an excited parent nucleus, with nucleon emission, to a variety of energy levels in the excited daughter nucleus. The parent can be excited to a variety of energies because the projectile nucleus brings in a variety of incident photon energies. The energy of the emitted nucleon can vary.

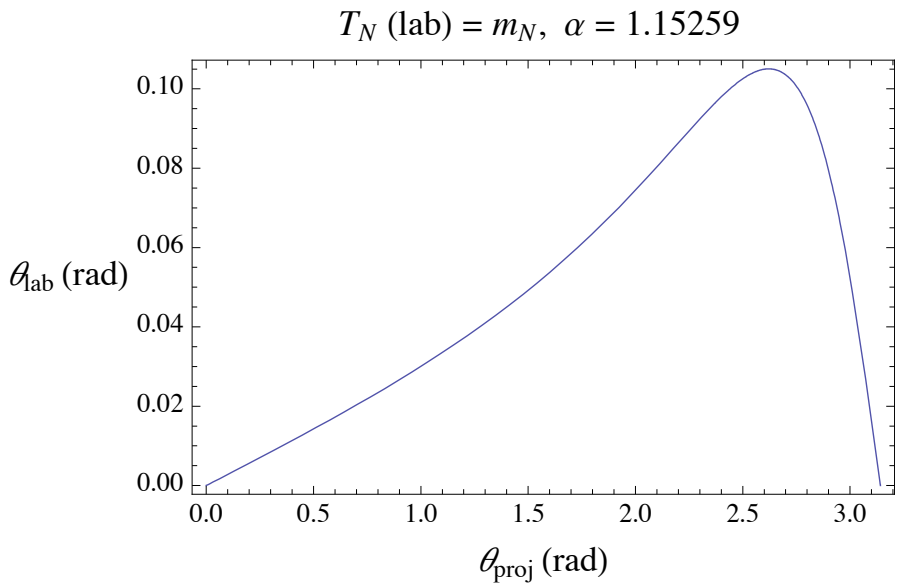

Figure 5: Relation between projectile and lab angles for an emitted photonucleon with kinetic energy $T_N = m_N$ or $\alpha = 1.15259$. The calculation used equation (67).

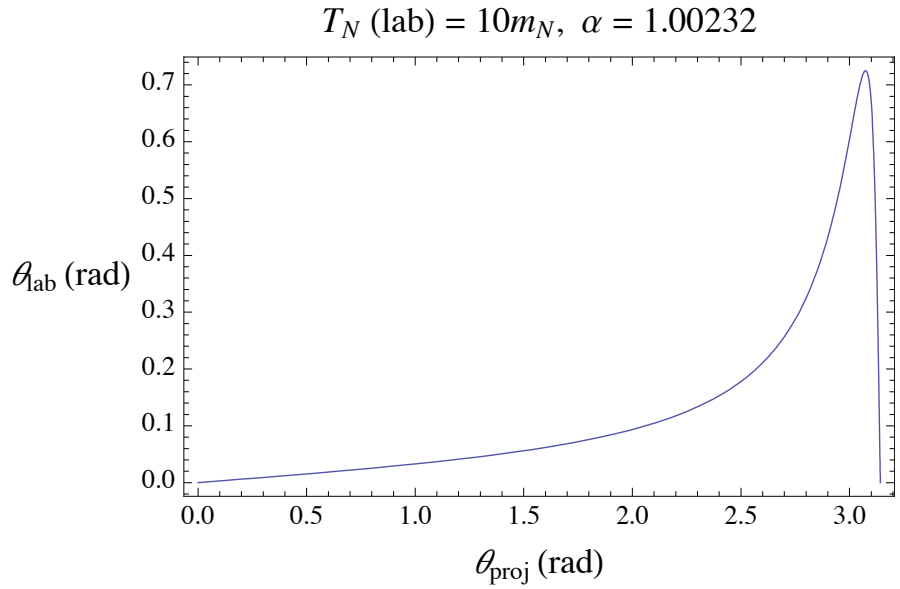

Figure 6: Relation between projectile and lab angles for an emitted photonucleon with kinetic energy $T_N = 10m_N$ or $\alpha = 1.00232$. The calculation used equation (67).

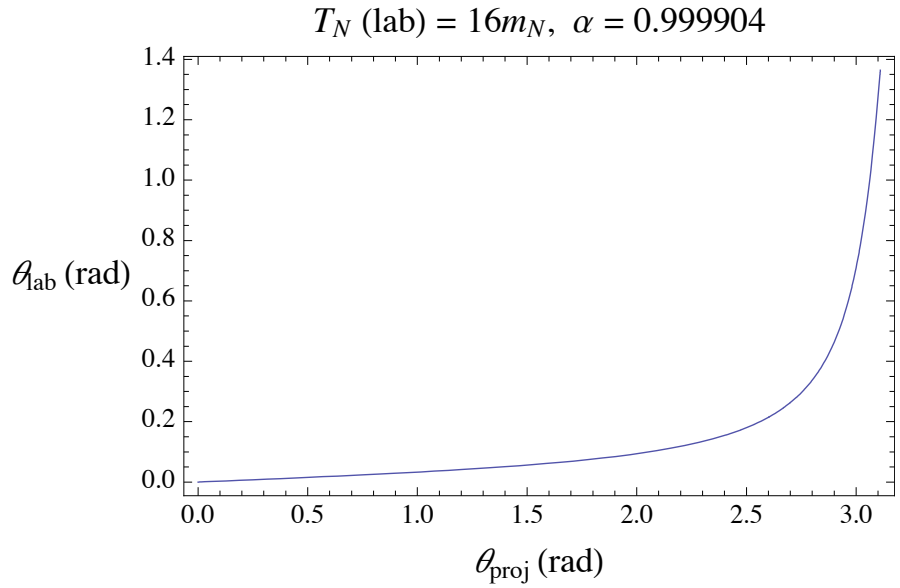

Figure 7: Relation between projectile and lab angles for an emitted photonucleon with kinetic energy $T_N = 16m_N$ or $\alpha = 0.999904$. The calculation used equation (67).

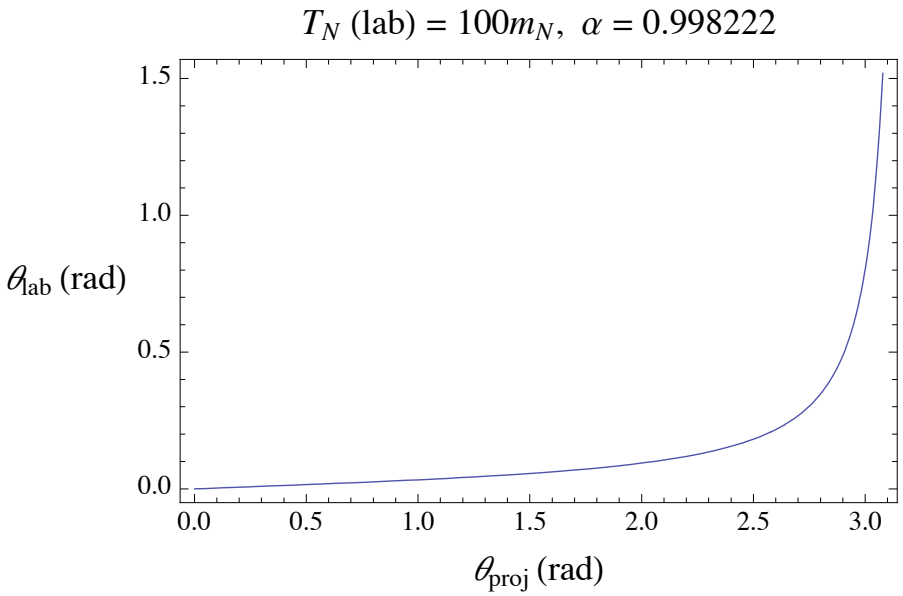

Figure 8: Relation between projectile and lab angles for an emitted photonucleon with kinetic energy $T_N = 100m_N$ or $\alpha = 0.998222$. The calculation used equation (67).

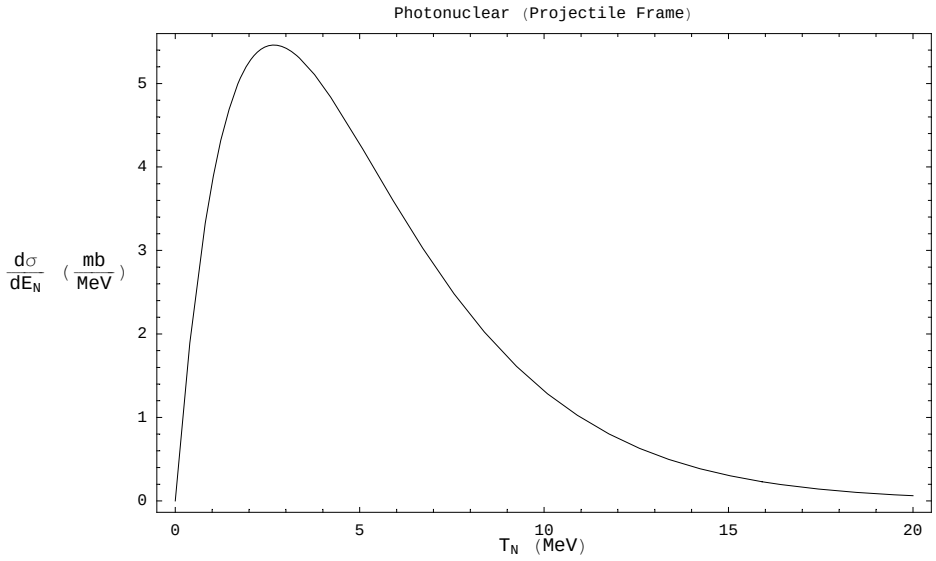

Figure 9: Photonuclear spectral distribution in the projectile frame evaluated at a photon energy of 20 MeV. The calculation was done using equation (14).

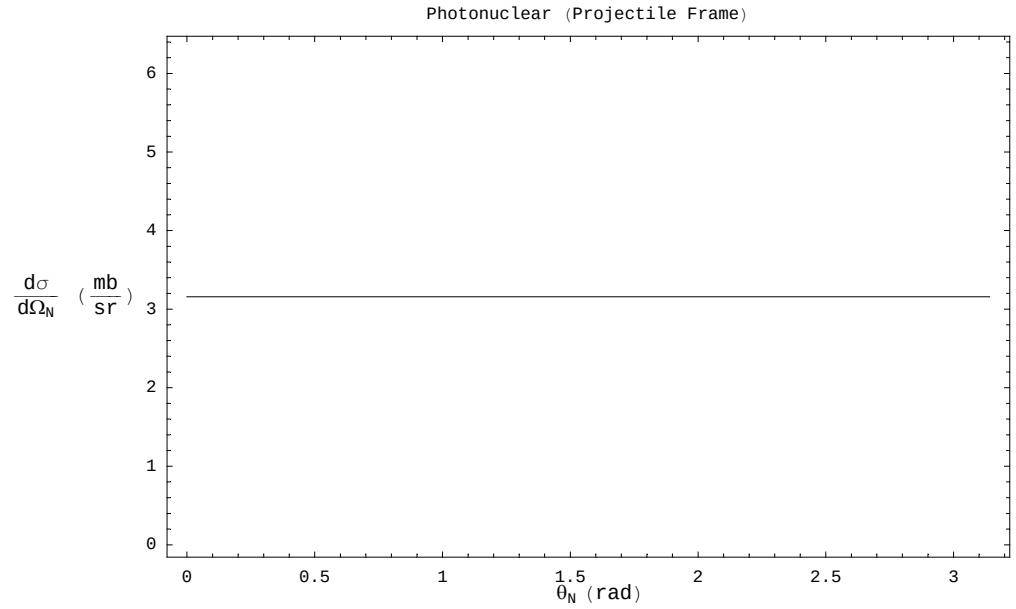

Figure 10: Photonuclear angular distribution in the projectile frame evaluated at a photon energy of 20 MeV.

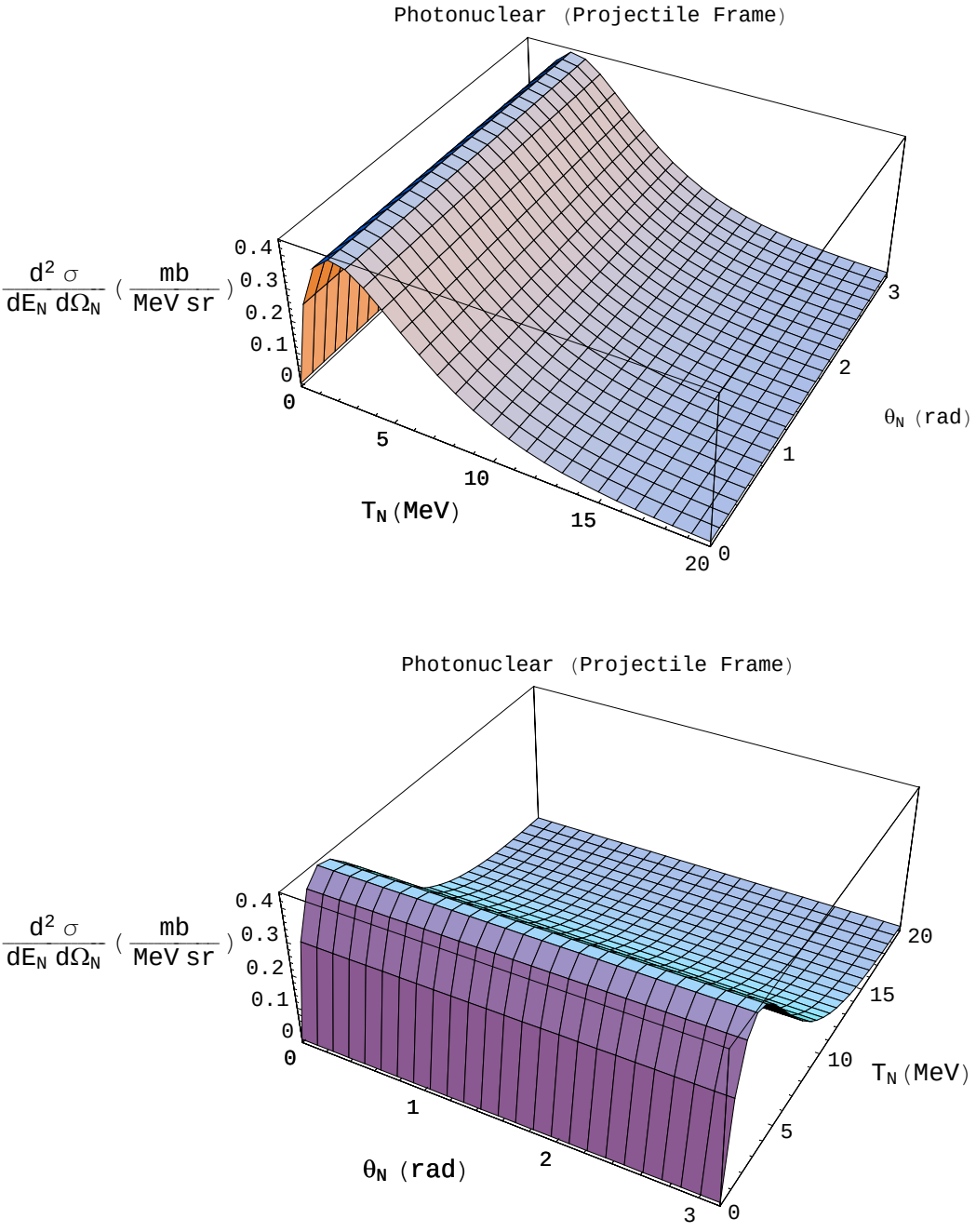

Figure 11: Photonuclear double differential cross section in the projectile frame evaluated at a photon energy of 20 MeV. (Bottom figure is same as top figure, except rotated.) The calculation was done using equation (29).

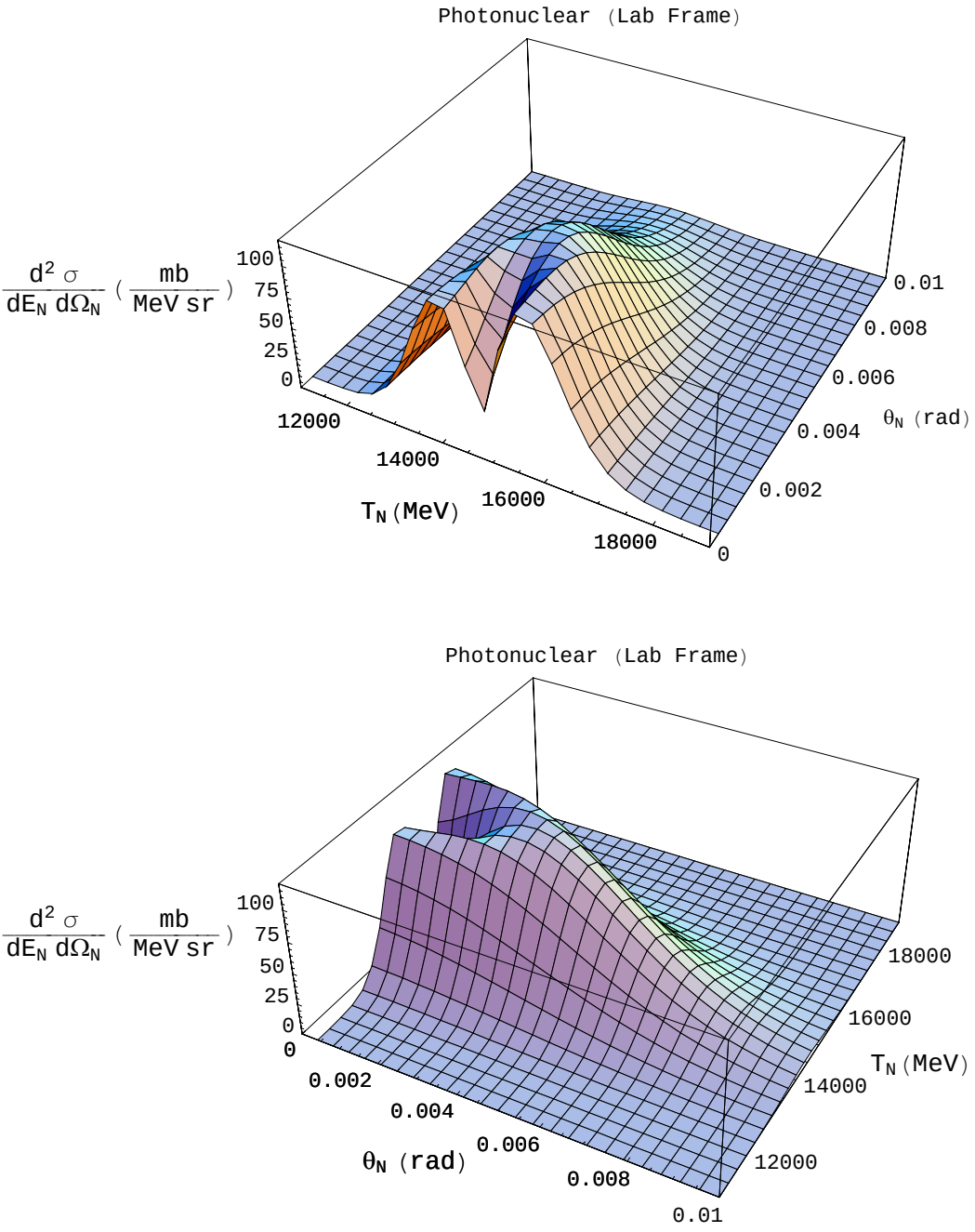

Figure 12: Photonuclear double differential cross section in the lab frame evaluated at a photon energy of 20 MeV. (Bottom figure is same as top figure, except rotated.) The calculation was done using equation (72).

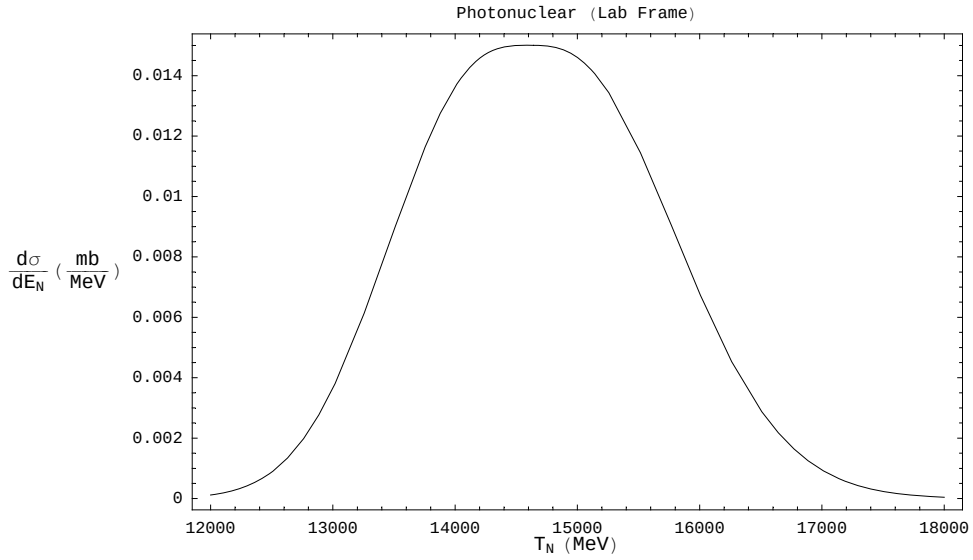

Figure 13: Photonuclear spectral distribution in the lab frame evaluated a photon energy of 20 MeV. The calculation was done using equation (72) and integrating over the angle.

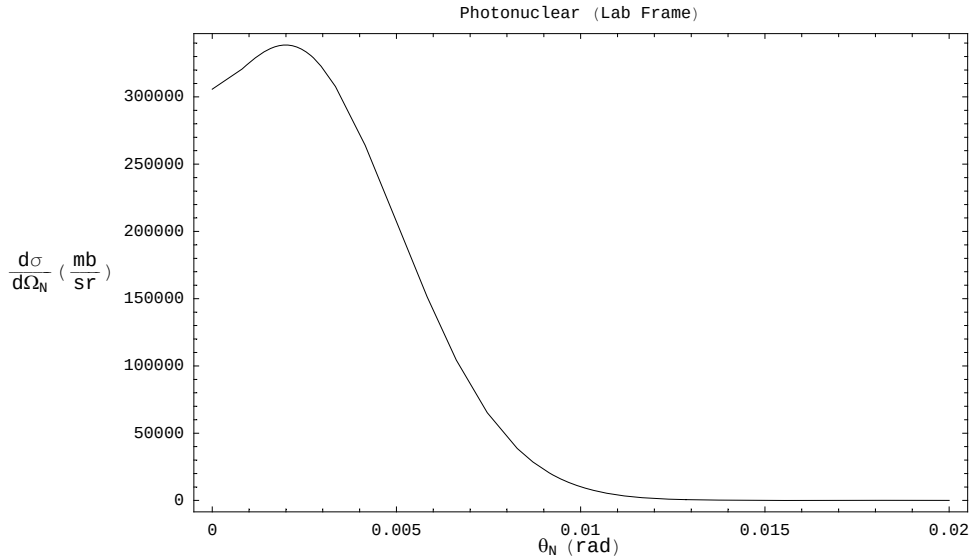

Figure 14: Photonuclear angular distribution in the lab frame evaluated at a photon energy of 20 MeV. The calculation was done using equation (72) and integrating over energy.

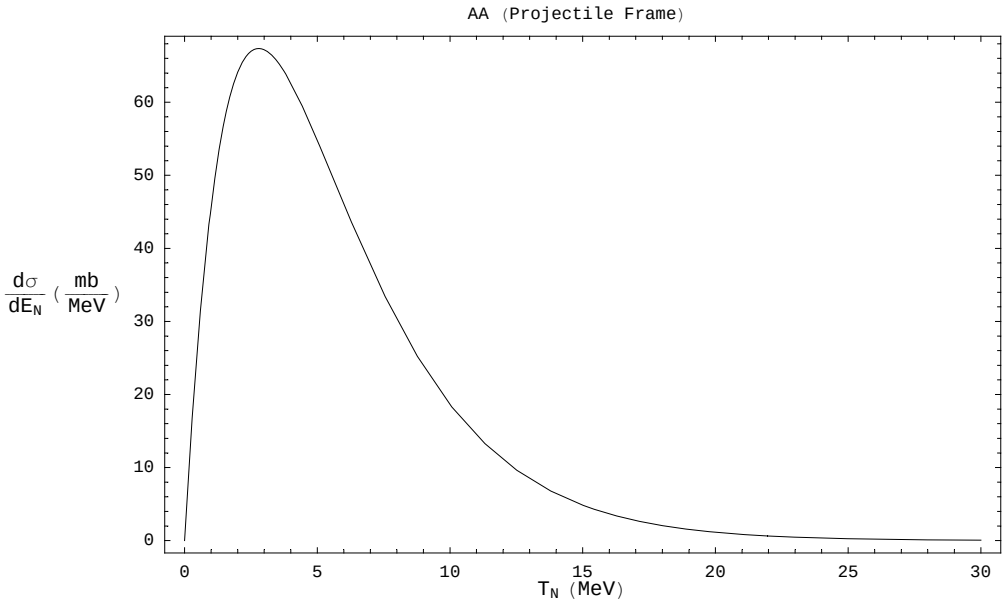

Figure 15: Nucleus - nucleus spectral distribution in the projectile frame. The calculation was done using equation (47).

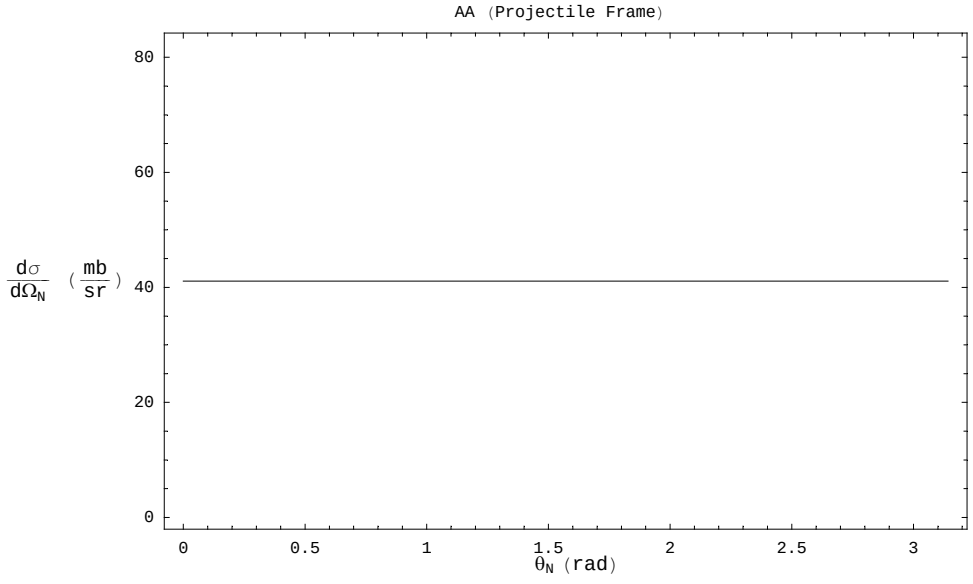

Figure 16: Nucleus - nucleus angular distribution in the projectile frame.

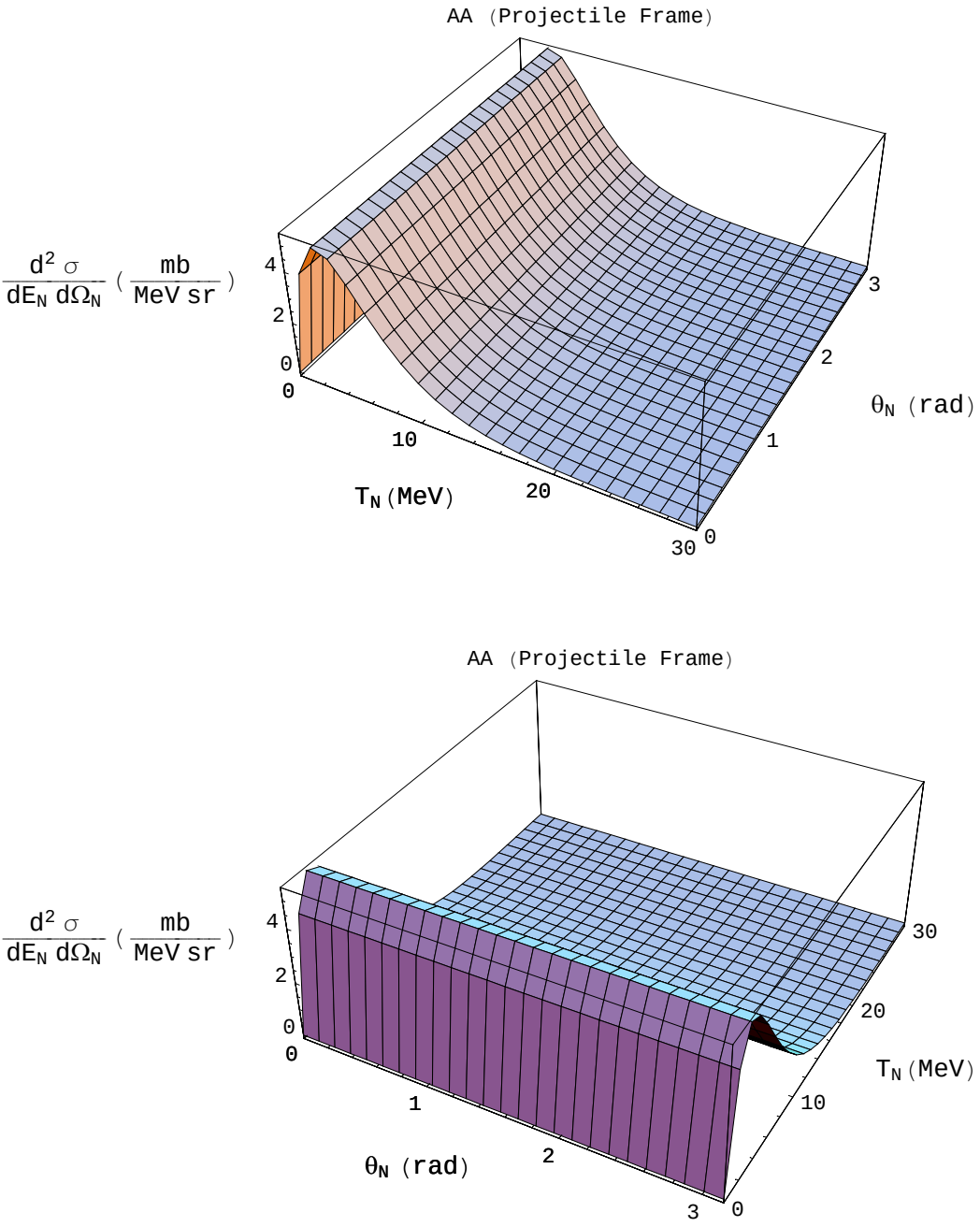

Figure 17: Nucleus - nucleus double differential cross section in the projectile frame. (Bottom figure is same as top figure, except rotated.) The calculation was done using equation (48).

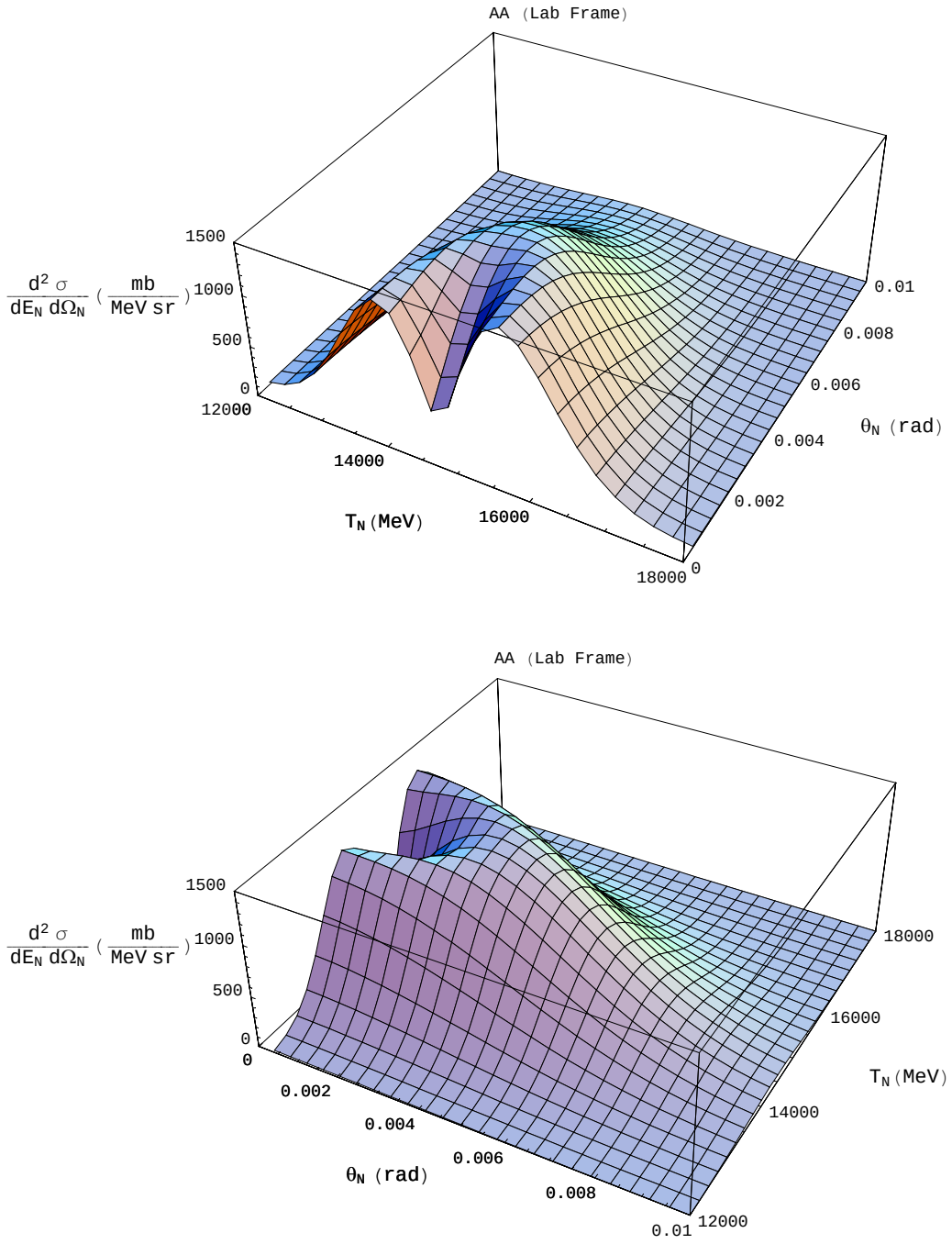

Figure 18: Nucleus - nucleus double differential cross section in the lab frame. (Bottom figure is same as top figure, except rotated.) The calculation was done using equation (48) and by transforming to the lab frame.

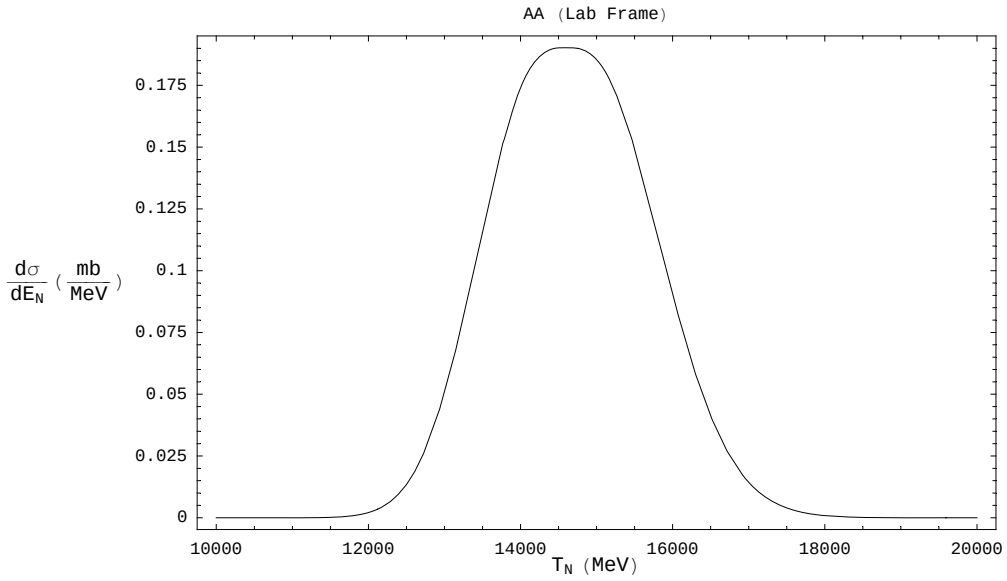

Figure 19: Nucleus - nucleus spectral distribution in the lab frame. The calculation was done using equation (48) and by transforming to the lab frame, and integrating over the angle.

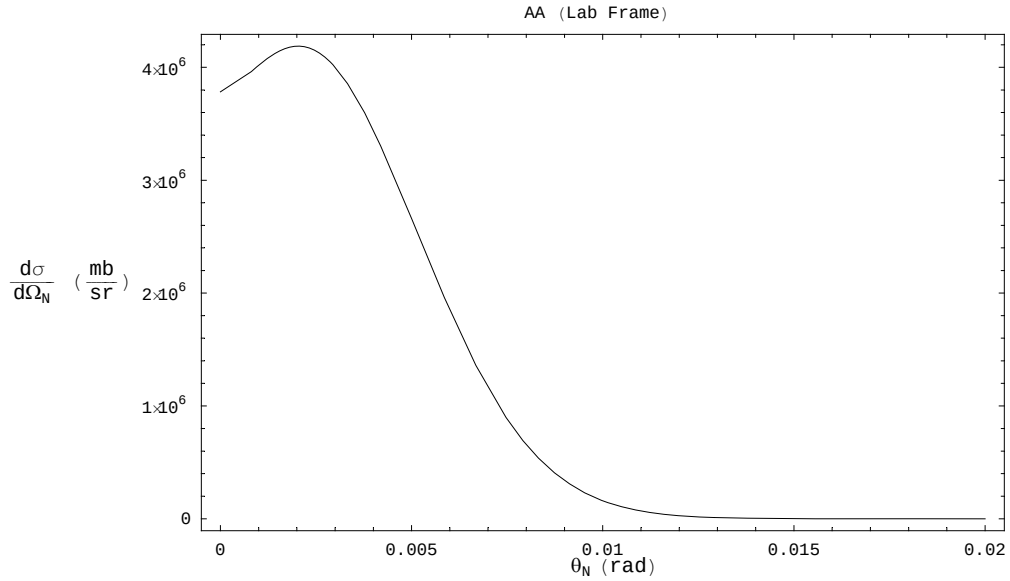

Figure 20: Nucleus - nucleus angular distribution in the lab frame. The calculation was done using equation (48) and by transforming to the lab frame, and integrating over the energy.

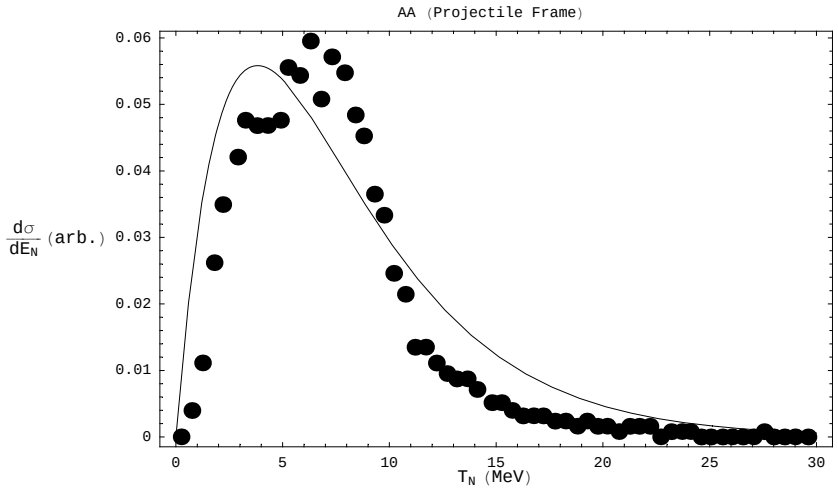

Figure 21: Comparison between theory and experiment for proton kinetic energy distribution in the projectile frame. The reaction is $^{28}Si + Pb \rightarrow 1p + ^{27}Al + Pb$ at 14.6 A GeV. Cross section units are arbitrary. Experimental data are from figure 13(b) of reference [40] and are represented by the large dots. Error bars are smaller than symbol sizes.

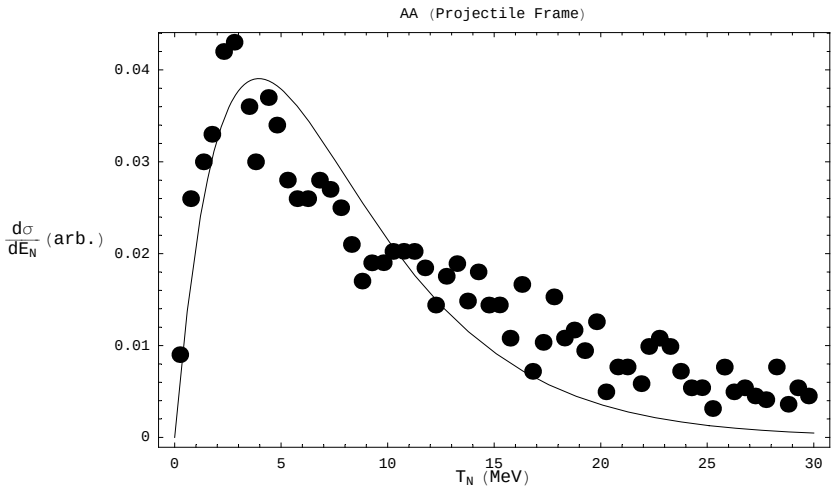

Figure 22: Comparison between theory and experiment for neutron kinetic energy distribution in the projectile frame. The reaction is $^{28}Si + Pb \rightarrow 1n + ^{27}Si + Pb$ at 14.6 A GeV. Experimental data are from figure 13(c) of reference [40] and are represented by the large dots. Cross section units are arbitrary. Error bars are smaller than symbol sizes.

REPORT DOCUMENTATION PAGE

Form Approved
OMB No. 0704-0188

1. REPORT DATE *(DD-MM-YYYY)*	2. REPORT TYPE	3. DATES COVERED *(From - To)*
01- 10 - 2008	Technical Publication	

4. TITLE AND SUBTITLE
Projectile and Lab Frame Differential Cross Sections for Electromagnetic Dissociation

5a. CONTRACT NUMBER

5b. GRANT NUMBER

5c. PROGRAM ELEMENT NUMBER

6. AUTHOR(S)
Norbury, John W.; Adamczyk, Anne; and Dick, Frank

5d. PROJECT NUMBER

5e. TASK NUMBER

5f. WORK UNIT NUMBER
651549.02.07.01

7. PERFORMING ORGANIZATION NAME(S) AND ADDRESS(ES)
NASA Langley Research Center
Hampton, VA 23681-2199

8. PERFORMING ORGANIZATION REPORT NUMBER
L-19383

9. SPONSORING/MONITORING AGENCY NAME(S) AND ADDRESS(ES)
National Aeronautics and Space Administration
Washington, DC 20546-0001

10. SPONSOR/MONITOR'S ACRONYM(S)
NASA

11. SPONSOR/MONITOR'S REPORT NUMBER(S)
NASA/TP-2008-215534

12. DISTRIBUTION/AVAILABILITY STATEMENT
Unclassified - Unlimited
Subject Category 93
Availability: NASA CASI (301) 621-0390

13. SUPPLEMENTARY NOTES

14. ABSTRACT
Differential cross sections for electromagnetic dissociation in nuclear collisions are calculated for the first time. In order to be useful for three - dimensional transport codes, these cross sections have been calculated in both the projectile and lab frames. The formulas for these cross sections are such that they can be immediately used in space radiation transport codes. Only a limited amount of data exists, but the comparison between theory and experiment is good.

15. SUBJECT TERMS
Electromagnetic dissociation; Space radiation

16. SECURITY CLASSIFICATION OF:			17. LIMITATION OF ABSTRACT	18. NUMBER OF PAGES	19a. NAME OF RESPONSIBLE PERSON
a. REPORT	b. ABSTRACT	c. THIS PAGE			STI Help Desk (email: help@sti.nasa.gov)
					19b. TELEPHONE NUMBER *(Include area code)*
U	U	U	UU	42	(301) 621-0390